A theory-guided probabilistic machine learning framework for accelerated prediction of process-induced deformations in advanced composites

A THEORY-GUIDED PROBABILISTIC MACHINE LEARNING FRAMEWORK FOR ACCELERATED PREDICTION OF PROCESS-INDUCED DEFORMATIONS IN ADVANCED COMPOSITES

Caleb Schoenholz [1,a], Enrico Zappino [2,b], Marco Petrolo [2,c], Navid Zobeiry [1,d,*]

[1] Materials Science & Engineering Department, University of Washington, 302 Roberts Hall, Box 352120, Seattle, WA, 98195-2120, U.S.A.
Email: [a] css1119@uw.edu, [d] navidz@uw.edu, Web Page: https://composites.uw.edu/

[2] MUL2 Lab, Department of Mechanical and Aerospace Engineering, Politecnico di Torino, Corso Duca degli Abruzzi 24, 10129 Torino, Italy
Email: [b] enrico.zappino@polito.it, [c] marco.petrolo@polito.it, Web Page: http://www.mul2.polito.it/

[*] Corresponding Author

Keywords: Aerospace composites manufacturing, process-induced deformations (PIDs), theory-guided probabilistic machine learning, Carrera Unified Formulation (CUF)

Abstract
This paper introduces an innovative framework for efficient analysis of composites manufacturing processes and phenomena. The method combines sparse probabilistic characterizations, multi-fidelity simulation schemes, and limited experiments to train surrogate machine learning (ML) models. Guided by a probabilistic technique, Spatially Weighted Gaussian Process Regression (SWGPR), predictive models are constructed from multi-fidelity data to perform rapid and accurate manufacturing assessments. This study demonstrates the effectiveness of the framework in accurately predicting process-induced deformations (PIDs) for L-shaped composite parts using minimal experimental efforts. The method introduced in this work aims to offer a cost-efficient and broadly applicable framework for potentially mitigating PIDs and solving other composites manufacturing problems.

1. Introduction

While carbon fiber-reinforced polymer (CFRP) composites have seen widespread use throughout the aerospace industry, manufacturers continue to face several challenges. One such challenge is the prediction and control of process-induced deformations (PIDs) in composite parts [1–3]. During autoclave processing, residual stresses form due to complex material and manufacturing phenomena [3]. Upon demolding, some of these stresses may be released through deformations such as angle alterations at transition points (e.g., spring-in) or warping of initially flat sections, as schematically illustrated in Figure 1 [4]. Consequently, these PIDs may induce joining gaps during assembly, prolong production timelines, and compromise the final structure's mechanical efficiency [5].

Despite having a general understanding of PIDs, manufacturers often struggle to accurately predict deformations in composite parts. These difficulties primarily stem from limitations of traditional prediction methods, typically classified into three categories: low-fidelity simulation (e.g., 1D/2D FE), high-fidelity simulation (e.g., 3D FE), and experimentation. One of the most notable constraints in these methods is the trade-off between fidelity/accuracy and time/cost [6], [7]. To address this trade-off, one common approach entails generating a relatively large simulation dataset alongside a smaller experimental dataset. Efforts are then made to calibrate the simulation data or its framework by linking the virtual and real-world domains using deterministic techniques (e.g., least-squares). However, due to

challenges and costs associated with acquiring large data, the virtual-to-real linkage and calibration attempts often rely on inadequate data, resulting in imprecise manufacturing evaluations.

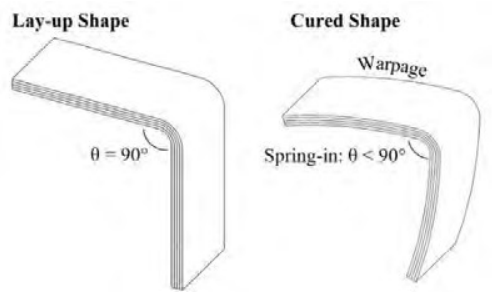

Figure 1. Schematic example of process-induced deformations (PIDs) in an L-shaped composite part.

Given the challenges previously discussed, there exists an opportunity to explore alternative methods for more efficient analysis of composites processing. This paper presents a versatile framework for this purpose, building upon recent research [6] and following the subsequent workflow for a case study on PIDs of L-shaped composite parts made from Toray's T800S/3900-2B material system. First, the evolution of select thermo-mechanical properties are characterized using a limited amount of Dynamic Mechanical Analysis (DMA) testing and the probabilistic machine learning technique, Gaussian Process Regression (GPR). The surrogate material property models are then utilized as inputs in a low-fidelity finite element (FE) simulation scheme to efficiently compute PIDs for composite parts within a design space. The low-fidelity virtual data is then mapped to theory-guided domains and utilized to train additional GPR models that predict PIDs. Next, these GPR models are iteratively calibrated by incorporating high-fidelity 3D simulation data and limited experimental data. In each retraining iteration, simulation data is assigned point-specific noises based on a Gaussian distance-decay weighing mechanism, creating a probabilistic model with a data-driven uncertainty structure. The method introduced in this work offers an alternative and flexible framework for solving problems and potentially mitigating PIDs in composite parts.

2. Material and Methods

2.1. Process Specifications

In this section, we outline the processing conditions for the case study evaluated in this work. The composite material utilized was Toray T800S/3900-2B unidirectional (UD) prepreg with a resin weight content of 35.5%, a primary structural material in major aircraft such as the Boeing 787 [8], [9]. Figure 2 illustrates the geometry and terminology used to characterize composite parts in this study. Prior to processing, each part had an L-shaped configuration with eight T800S/3900-2B plies, a flange length of 154.2 mm, a width of 50.8 mm, a corner radius of 15.875 mm, and a corner angle of 90°. All parts were processed according to the Manufacturer's Recommended Cure Cycle (MRCC) of heating to 180 °C at 2 °C/min, holding at 180 °C for 120 minutes, then cooling to room temperature at 2 °C/min. The curing process was conducted under a combined autoclave and vacuum pressure of approximately 0.7 MPa.

After curing and demolding, L-shaped parts may deform into a wide range of configurations with diverse spring-in and warpage magnitudes and directions (e.g., Figure 2) [6], [10]. In this study, positive spring-in values indicate angle enlargements between flanges, while negative values denote angle enclosures. Similarly, positive and negative warpages represent concave-down and concave-up flange distortions, respectively. The maximum warpage (w_{max}) for each part corresponds to the greatest absolute out-of-plane deformation along the flange. In this study, the 1 and 0° directions represent the longitudinal fiber orientation, while 2 and 90° denote the transverse fiber orientation, and 3 pertains to the out-of-plane

fiber dimension. Finally, directions x, y, and z signify the longitudinal, transverse, and out-of-plane dimensions of the L-shaped laminates.

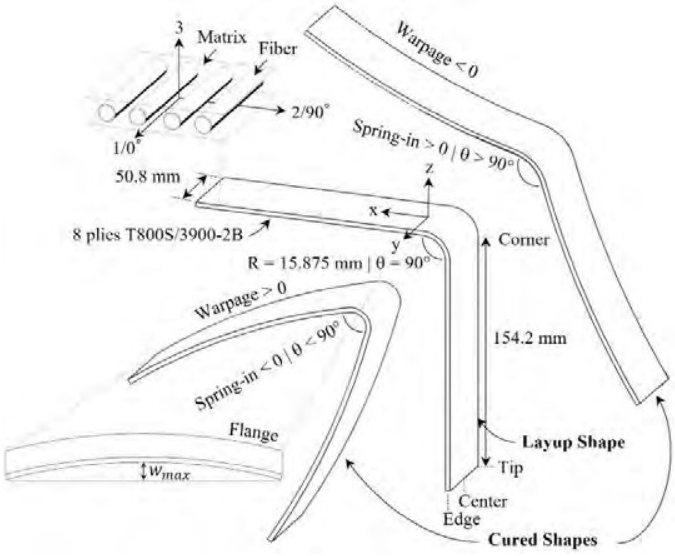

Figure 2. Geometry and terminology used to characterize L-shaped composite parts.

2.2. Low-fidelity Simulation

In this section, we outline a low-fidelity numerical model employed to predict PIDs in L-shaped parts. Inspired by Takagaki et al.'s analytical approach [11], the model uses the in-situ shear and bending moduli of a laminate, free strains during the curing process, and geometric parameters of L-shaped parts as inputs to estimate incremental stresses and deformations during processing. In this work, input properties were obtained by simulating the degree of cure (DoC) and glass transition temperature (T_g) of the composite using Dykeman's model [12], then computing thermo-mechanical properties using surrogate models from bi-material beam (BMB) testing, as outlined in Section 2.4.1. [13]. The Cure Hardening Instantaneously Linear Elastic (CHILE) assumption was then applied to predict the final corner spring-in, tip spring-in, and maximum warpage of the L-shaped parts [14]. The entire curing and deformation analysis was performed using a custom Python [15] code. An overview of the thermo-mechanical equations and algorithms employed in the code can be referenced in [6].

2.3. High-fidelity Simulation

This section provides a concise overview of a high-fidelity simulation approach employed for predicting PIDs, while more comprehensive details are available in [16]. The high-fidelity framework utilizes a refined 1D kinematic model based on the Carrera Unified Formulation (CUF) [17], [18] and CHILE assumptions [14], enabling efficient layer-wise (LW) modeling and precise 3D representations of residual stresses and PIDs. The model incorporates bending and shear moduli (E and G), Poisson's ratio (ν), coefficient of thermal expansion (α), and cure shrinkage-induced strain ($\Delta\varepsilon_{cs}$) in each of the three principal directions, sourced from published literature and a BMB validation test [9], [12], [16], [19]. Following each high-fidelity simulation, geometric analyses were conducted to derive corner spring-in, tip spring-in, and maximum warpage at the center and edge of each laminate.

2.4. Experimentation

2.4.1. Thermo-mechanical Characterization

This section summarizes the procedures used to characterize thermo-mechanical properties for inputs into the low-fidelity simulation scheme. The characterization was achieved through a bi-material beam (BMB) test in a TA Instruments Dynamic Mechanical Analyzer (DMA) 850 [3], [13]. The experimental setup involved a 12.7 mm (w) × 60 mm (l) beam with four layers of 90-degree prepreg bonded on top of a steel shim, supported by a 3-point bend fixture in the DMA. Additionally, a small hole was cut through all the prepreg layers in the center of the beam, and a steel ball was placed in the hole atop the steel shim.

During DMA testing, the BMB specimen was subjected to a temperature cycle, a static force of 0.1 N, and a continuous sinusoidal displacement with an amplitude and frequency of 150 μm and 0.1 Hz, respectively [13]. The DMA measured the applied force, displacement, and phase angle at discrete time steps, which were then used to calculate the evolution of the beam's effective stiffness and the prepreg's storage modulus using available closed-form solutions [13]. Lastly, the computed modulus values were combined with pseudo viscoelastic (PVE) Laminated Plate Theory (LPT) and the measured out-of-plane beam deflection (i.e., cure shrinkage- and thermal-induced) to determine free strain evolutions in the prepreg throughout the curing process [2], [20], [21].

2.4.2. Composites Manufacturing

This section outlines the procedures employed to generate experimental PID data. The process involved manufacturing L-shaped parts utilizing an autoclave, followed by quantifying PIDs using laser profilometry. A 6.35 mm-thick A-36 steel tool covered with a layer of fluorinated ethylene propylene (FEP) release film served as the layup mold. Three parts with dimensions specified in Figure *2* were evenly laid up across the width of the tool, vacuum sealed using standard bagging procedures, then placed in an autoclave and subjected to the MRCC. Then, the cured L-shaped parts were demolded from the tool and 2D spatial profiles were acquired at three locations utilizing a Keyence LJ-X8400 laser scanner. Schematic illustrations detailing the layup and laser scanning procedures can be found in [10]. After obtaining the scans, the profiles were superposed onto plots displaying the premeasured tool profile at the corresponding location and a custom Python [15] code was utilized to extract spring-in and warpage values at the center and edges of each part.

2.5. TGML Methodology

In this section, we outline a framework for the efficient analysis of composites manufacturing and prediction of PIDs. The methods presented here extend recent research [6], where more comprehensive details are provided. The main objective of this study is to further enhance predictive efficiency through the inclusion of a sparse characterization phase. The effectiveness of the approach will be evaluated through a case study focused on predicting PIDs for L-shaped parts with eight-ply layups consisting solely of zero- and ninety-degree plies.

The prediction process (Figure 3) starts with characterizing the evolution of the composite's thermo-mechanical properties solely under the processing conditions of interest, which in this study is the MRCC [9]. After completing a BMB test (Section 2.4.1.) under MRCC conditions, the probabilistic machine learning technique, Gaussian Process Regression (GPR), is used to train models for predicting the composite's dynamic modulus and free strains throughout the cure cycle [22]. Once the modulus and free strain models are trained, the fastest available data source (i.e., low-fidelity simulation) is employed to generate virtual PID data, including all nine elements of the extensional (A), coupling (B), and bending (D) stiffness matrices, tip spring-in, corner spring-in and maximum warpage for all 2^8 = 256 cross-ply laminations [11], [23].

Following the creation of the low-fidelity dataset, optimal feature representations (i.e., input parameters) for the laminates are defined, where the objective is to obtain similar input parameters yielding comparable PID outputs (i.e., smoothness). To achieve this, we utilize stiffness coefficients obtained

from low-fidelity simulations as inputs [10]. As prior studies have established connections between CLPT and PIDs [11], [24], [25], utilizing stiffness coefficients aims to offer physics-based guidance to the model and enhance its accuracy, forming the basis of our "theory-guided" machine learning framework.

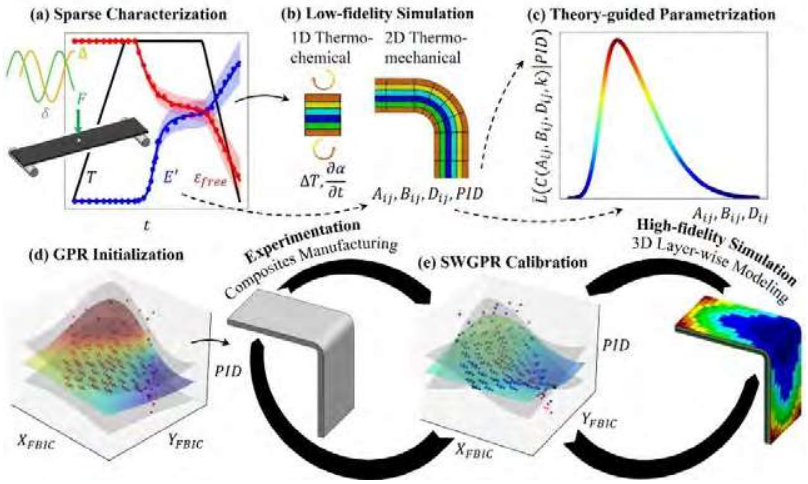

Figure 3. Flowchart of efficient composites manufacturing analysis method using sparse characterization, multi-fidelity simulation, and theory-guided machine learning.

Since training a model with a large input-to-output ratio presents several challenges, stiffness coefficients must be refined to an optimal number. In this work, the refinement is achieved using the Focused Bayesian Information Criterion (FBIC) [6], which evaluates input subsets by maximizing the likelihood function on training data while penalizing the number of parameters and computational time required for model fitting:

$$FBIC = -2\ln(\hat{L}) + kt\ln(n) \tag{1}$$

where $\hat{L}$ is the model's maximized likelihood function, k is the number of parameters, n is the number of datapoints, and t is the model's computational training time. To effectively employ (1), we first apply the constraint $k = 3$, limiting evaluations to two-input subsets and enabling the models to be visualizable as 3D surfaces. GPR models are then trained on all possible subsets (e.g., A_{11} and B_{22}) to predict low-fidelity simulated PIDs [26]. Subsequently, the FBIC is computed for each GPR model and the most optimal (i.e., lowest) subsets for each PID type are determined.

After constructing GPR models, a calibration process begins by iteratively substituting low-fidelity simulation data with high-fidelity simulation and experimental data (Figure 3e). The key assumption of this phase is that certain simulation data may be detrimental to the model's accuracy due to numerical simplifications, while experimental data will exclusively enhance GPR performance. To incorporate these assumptions, noise levels are assigned to the model's simulation data based on their proximity to experiments in the design space following:

$$w_{ij} = e^{-d_{ij}^2/2(h\times d_{ij,max})^2} \tag{2}$$

$$\alpha_{ij} = \ln(1/w_{ij}) \tag{3}$$

$$f(x) \sim \mathcal{GP}(m(x), k(x,x') + \alpha(d)I) \tag{4}$$

where w_{ij} is the weight of each lower-fidelity (i.e., simulation) datapoint, d_{ij} is the Euclidean distance between a lower-fidelity and experiment, h is a decay factor reflecting the uncertainty in a data source, $d_{ij,max}$ is the maximum distance between two datapoints in the domain, α_{ij} is the variance of Gaussian noise surrounding a datapoint, $f(x)$ is a function to be predicted, $\mathcal{GP}$ is the Gaussian Process, $m(x)$ is the mean function, $k(x, x')$ is the kernel function, $\alpha(d)$ is an array of distance-dependent noise levels, and I is the identity matrix. During model fitting, α values determined from h and d_{ij} are added to the kernel matrix's diagonal, introducing point-specific noise to each simulation datapoint. This establishes a multi-scale uncertainty structure, enabling GPR to treat multi-fidelity points differently, placing greater "trust" in and near experiments while mitigating the impact of "bad" virtual data. In other words, a GPR model with a spatially weighted uncertainty structure is established, as illustrated in Figure 4.

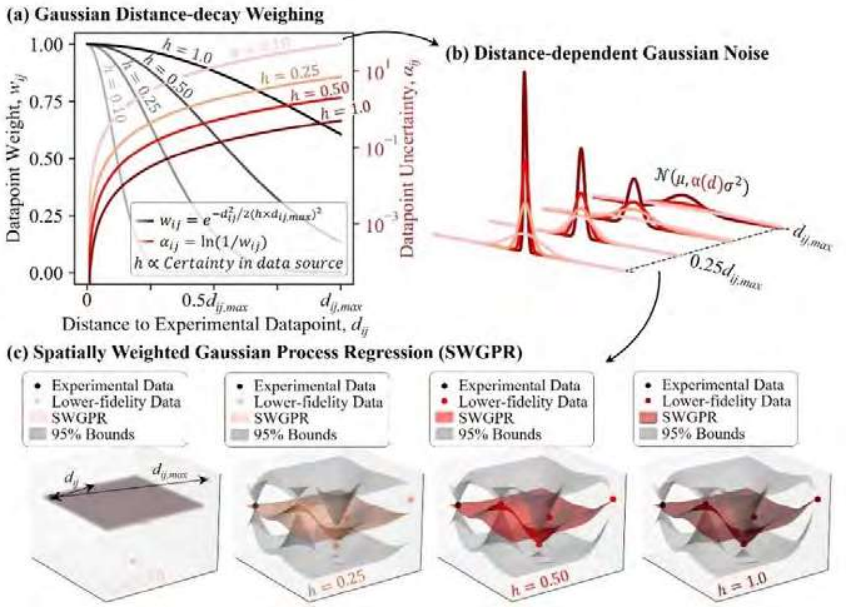

Figure 4. (a) Gaussian distance-decay weight and uncertainty, (b) Gaussian noise, and (c) SWGPR predictions for different low-fidelity uncertainty levels.

In this work, we define h values for each virtual data source as equal to the inverse of the number of material properties used as inputs: h = 1/3 = 0.33 for low-fidelity and h = 1/15 = 0.07 for high-fidelity simulation. Subsequently, the TGML prediction scheme progresses to its final phase (Figure 3e), where an experiment with parameters surrounded by the highest uncertainty is conducted and substituted for its corresponding low-fidelity datapoint, while other virtual points are weighed per (2) and (3). The SWGPR model is then retrained to predict PIDs and identify new locations with the highest uncertainty. Next, the parameters for which SWGPR is most uncertain are fed into the high-fidelity simulation scheme, PIDs are predicted, and the model is retrained. If the addition of high-fidelity simulation data improves accuracy, the process repeats with the high-fidelity simulation scheme. However, if accuracy remains unchanged or decreases, the process halts and another experiment is added to the model. The high-fidelity simulations may then be reinstated until its next accuracy plateau or until the model meets accuracy requirements. In this study, SWGPR accuracy is evaluated at each calibration step by comparing its predictions to experimental PID values from six testing laminates with diverse layups [6].

3. Results and Discussions

In this section, we illustrate the training of an SWGPR model using the TGML approach initiated by a sparse probabilistic characterization phase. We employ the method to predict the tip spring-in at the

center of six L-shaped composite parts with various cross-ply layups, as described in [6]. Subsequently, we evaluate the effectiveness of the supplementary sparse characterization phase by comparing the calibration efficiency to that of the original method, which initiated with extensive deterministic characterizations.

Figure 5 shows an SWGPR model and its predictions for tip spring-in of L-shaped laminates (a) before and (b) after undergoing calibration. In the left-side plots, red points are low-fidelity simulation data generated using a single BMB test and surrogate GPR modulus and free strain models, blue squares are high-fidelity simulations, and black stars are experiments used for model training. Multi-colored surfaces represent the SWGPR models' mean predictions, while grey surfaces are 95% confidence bounds. Tip spring-in is plotted against B_{11} and D_{22}, identified as optimal parameters using the FBIC. On the right side of the figure, tip spring-in predictions for the six testing laminates [6] are displayed, with black outlined bars indicating average experimental values and error bars representing standard deviations. Table 1 compares the performance and efficiency of the SWGPR calibration process with initiating with sparse probabilistic characterization with that of [6].

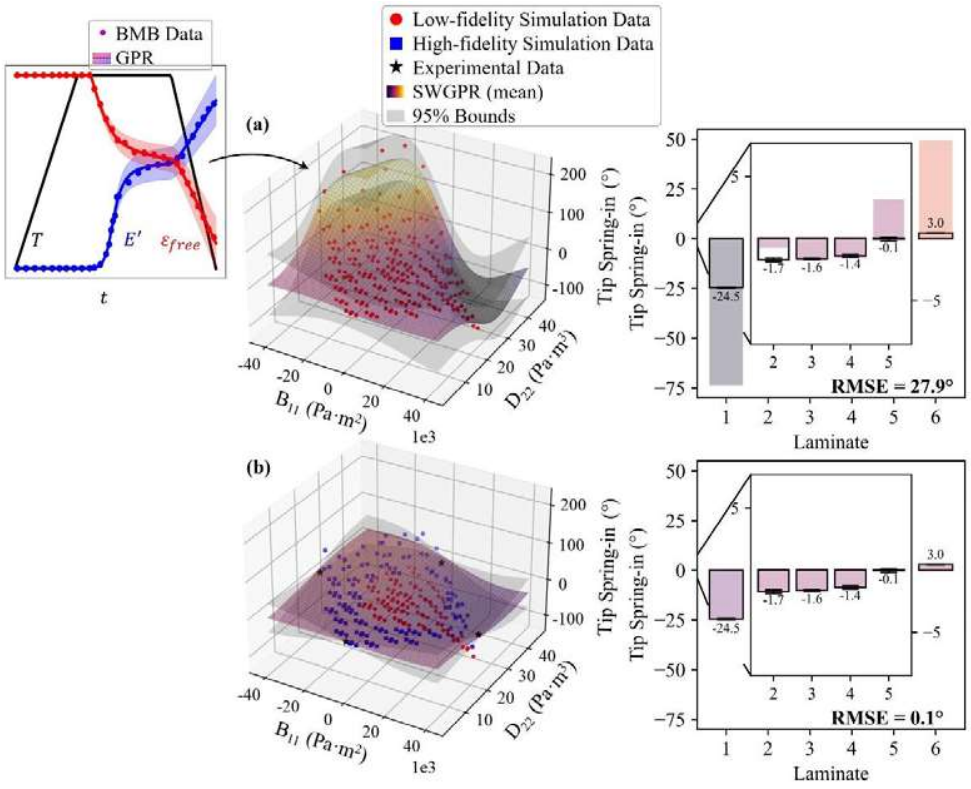

Figure 5. SWGPR model (a) before and (b) after calibration and its predictions of tip spring-in for L-shaped composite parts.

Initially, the SWGPR model, trained on 256 low-fidelity simulations derived from a single BMB test and the fitted GPR model under MRCC conditions, displayed a root mean squared error (RMSE) of 27.9° in predicting tip spring-in for the six testing laminates. Although this RMSE was slightly greater than that reported in [6], generating low-fidelity simulation data in this work required less than 10% of the testing time. These findings suggest that comparable accuracies can be attained by focusing on characterizing only the pertinent properties relevant to the specific case study, rather than investing

substantial time in fitting deterministic models. Following calibration, both SWGPR models, with and without sparse characterization, achieved convergence and accuracy requirements with only four experiments. Overall, the outcomes depicted in Figure 5 and Table 2 underscore the potential benefits of characterizing only essential thermo-mechanical properties, highlighting time-saving advantages and prompting further exploration in future research.

Table 1. Performance and efficiency of TGML-SWGPR methodologies.

	Pre-calibration		Post-calibration	
Characterization Method	RMSE (%)	Characterization Time (hr)	RMSE (%)	Experiments Required
Sparse Probabilistic	27.9	8	0.1	4
Deterministic [6]	27.7	204	0.1	4

4. Summary and Conclusions

This study introduced an innovative framework for efficient analysis of composites manufacturing using sparse probabilistic characterization, multi-fidelity simulation, limited experimentation, and theory-guided machine learning (TGML). It begins with a low-fidelity simulation approach utilizing material property models derived from Gaussian Process Regression (GPR) for rapid data generation. This data is then mapped to reduced-order theory-guided domains and iteratively calibrated using high-fidelity simulation data, experiments, and a spatial weighing mechanism. The strategies presented are highly efficient at predicting process-induced deformations (PIDs) in L-shaped composite parts and offer promise in advancing understanding in composites manufacturing.

Acknowledgments

This work was supported by Toray Composite Materials America, Inc. and by the project "An AI-assisted virtual manufacturing approach to mitigate defects in advanced composites" funded by the Italian Minister of Foreign Affairs and International Cooperation (MAECI) under grant number US23GR12.

References

[1] G. Fernlund, C. Mobuchon, and N. Zobeiry. *2.3 Autoclave Processing. Comprehensive Composite Materials II*. Elsevier, Amsterdam, 2018.
[2] N. Zobeiry, A. Forghani, C. Li, K. Gordnian, R. Thorpe, R. Vaziri, G. Fernlund, and A. Poursartip. Multiscale characterization and representation of composite materials during processing. *Philosophical Transactions of the Royal Society A: Mathematical, Physical and Engineering Sciences*, 374, 2016.
[3] N. Zobeiry and A. Poursartip. The origins of residual stress and its evaluation in composite materials. *Structural Integrity and Durability of Advanced Composites: Innovative Modelling Methods and Intelligent Design*. Woodhead Publishing, Cambridge, 2015.
[4] A. Albert and G. Fernlund. Spring-in and warpage of angled composite laminates. *Composites Science and Technology*, 62:1895–912, 2002.
[5] K. Manohar, T. Hogan, J. Buttrick, AG. Banerjee, JN. Kutz, and SL. Brunton. Predicting shim gaps in aircraft assembly with machine learning and sparse sensing. *Journal of Manufacturing Systems*, 48:87–95, 2018.
[6] C. Schoenholz, E. Zappino, M. Petrolo, and N. Zobeiry. Efficient analysis of composites manufacturing using multi-fidelity simulation and probabilistic machine learning. *Composites Part B: Engineering*, 280:111499, 2024.
[7] N. Zobeiry and A. Poursartip. Theory-Guided Machine Learning for Process Simulation of Advanced Composites, 2021.
[8] N. Odagiri, H. Kishi, and M. Yamashita. Development of TORAYCA prepreg P2302 carbon fiber reinforced plastic for aircraft primary structural materials. *Advanced Composite Materials*, 5:249–54, 1996.

[9] 3900 Prepreg System | Toray Composite Materials America, Inc. 2020.
[10] C. Schoenholz and N. Zobeiry. An Accelerated Process Optimization Method to Minimize Deformations in Composites Using Theory-guided Probabilistic Machine Learning. *Composites Part A: Applied Science and Manufacturing*, 176:107842, 2024.
[11] K. Takagaki, S. Minakuchi, and N. Takeda. Process-induced strain and distortion in curved composites. Part I: Development of fiber-optic strain monitoring technique and analytical methods. *Composites Part A: Applied Science and Manufacturing*, 103:236–51, 2017.
[12] D. Dykeman. Minimizing uncertainty in cure modeling for composites manufacturing. *Doctor of Philosophy, University of British Columbia*, 2008.
[13] R. Thorpe. Experimental characterization of the viscoelastic behavior of a curing epoxy matrix composite from pre-gelation to full cure. *Master of Applied Science. University of British Columbia*, 2013.
[14] N. Zobeiry, R. Vaziri, and A. Poursartip. Computationally efficient pseudo-viscoelastic models for evaluation of residual stresses in thermoset polymer composites during cure. *Composites Part A: Applied Science and Manufacturing*, 41:247–56, 2010.
[15] G. Van Rossum, and F. Drake Jr. Python. Version 3.10. 2021.
[16] E. Zappino, N. Zobeiry, M. Petrolo, R. Vaziri, E. Carrera, and A. Poursartip. Analysis of process-induced deformations and residual stresses in curved composite parts considering transverse shear stress and thickness stretching. *Composite Structures*, 241:112057, 2020.
[17] D. Scano, E. Carrera, and M. Petrolo. Use of the 3D Equilibrium Equations in the Free-Edge Analysis for Laminated Structures with the Variable Kinematics Approach. *Aerotecnica Missili & Spazio*, 1:1–17, 2023.
[18] E. Carrera, M. Cinefra, E. Zappino, and M. Petrolo. Finite Element Analysis of Structures through Unified Formulation. Wiley Blackwell, 9781119941217, 2014.
[19] C. Chen, A. Poursartip, and G. Fernlund. A novel method to measure laminate shear modulus development of interlayer toughened composite laminates during the curing process. In *Proceedings of the American Society for Composites - 34th Technical Conference*, 2019.
[20] C. Kassapoglou. *Design and Analysis of Composite Structures: With Applications to Aerospace Structures*. Second Edition, John Wiley & Sons, Ltd., West Sussex, United Kingdom, p. 189–236, 2013.
[21] C. Li, N. Zobeiry, K. Keil, S. Chatterjee, and A. Poursartip. Advances in the Characterization of Residual Stress in Composite Structures. In *International SAMPE Conference*, 2014.
[22] C. Rasmussen and C. Williams. Gaussian Processes for Machine Learning. The MIT Press, 2006.
[23] C. Kassapoglou. *Design and Analysis of Composite Structures: With Applications to Aerospace Structures*. Second Edition, John Wiley & Sons, Ltd., West Sussex, United Kingdom, p. 33–53, 2013.
[24] A. Arafath, R. Vaziri, and A. Poursartip. Closed-form solution for process-induced stresses and deformation of a composite part cured on a solid tool: Part II – Curved geometries. *Composites Part A: Applied Science and Manufacturing*, 40:1545–57, 2009.
[25] M. Wisnom, K. Potter, and N. Ersoy. Shear-lag Analysis of the Effect of Thickness on Spring-in of Curved Composites. *Journal of Composite Materials*, 41:1311–24, 2006.
[26] F. Pedregosa, G. Varoquaux, A. Gramfort, V. Michel, B. Thirion, O. Grisel, M. Blondel, P. Prettenhofer, R. Weiss, V. Dubourg, J. Vanderplas, A. Passos, D. Cournapeau, M. Brucher, M. Perrot, and E. Duchesnay. Scikit-learn: Machine Learning in Python. *Journal of Machine Learning Research*, 12:2825–30, 2011.